Original scientific paper
https://doi.org/10.33180/InfMIDEM2026.104

Informacije MIDEM
Journal of Microelectronics, Electronic Components and Materials
Vol. 56, No. 1(2026), 37 – 45

Effect of Li_3AlF_6 as Sintering-aids on the Structure and Conductivity of $Li_{0.25}La_{0.25}NbO_3$ Ceramic Solid Electrolytes

Yuxin Wang[1], Weiwei Hu[2], Zimeng Shi[1], Yazhou Kong[1], Yifei Chen[1], Mengyao Lu[1], Jie Chang[1], Guang Hu[1], Kailong Zhang[1], Jiangli Xiong[1], Jianfeng Pang[1]

[1]National & Local Joint Engineering Research Center for Mineral Salt Deep Utilization, Faculty of Chemical Engineering, Huaiyin Institute of Technology, Huaian, P.R. China
[2]Jiangsu Key Laboratory of Regional Specific Resource Pharmaceutical Transformation, Green Chemistry and Process Enhancement Technology, Huaiyin Institute of Technology, Huaian, China

Abstract: With the growing demand for high-safety and high-energy-density energy storage systems, all-solid-state lithium batteries (ASSLBs) have attracted extensive attention due to their excellent safety and potential high performance. Among them, the solid electrolyte is a key component. This study systematically investigates the effects of Li_3AlF_6 as a sintering aid on the sintering behavior, crystal structure, microstructure, and electrochemical performance of LLNO ($Li_{0.25}La_{0.25}NbO_3$) ceramics. LLNO ceramic samples with different Li_3AlF_6 doping levels (0-8 wt.%) were prepared via a solid-state reaction method and sintered at 1050 °C and 1100 °C. The samples were characterized by XRD, SEM, AC impedance spectroscopy, and DC polarization testing. The results indicate that Li_3AlF_6 significantly reduces the sintering temperature of LLNO and promotes the densification process. However, excessive doping (8 wt.%) leads to the formation of impurity phases such as AlF_3, increases grain boundary resistance, and reduces ionic conductivity. The sample with 5 wt.% Li_3AlF_6 sintered at 1050 °C exhibits the best overall performance: an ionic conductivity of 2.08×10^{-6} S·cm^{-1} and an activation energy of 0.340 eV. Although its conductivity is slightly lower than that of pure LLNO (4.12×10^{-6} S·cm^{-1}) sintered at 1100 °C, the introduction of Li_3AlF_6 provides a feasible route for low-temperature sintering, which is beneficial for future co-sintering integration with electrode materials.

Keywords: $Li_{0.25}La_{0.25}NbO_3$, Li_3AlF_6, Sintering aids, Ceramic

Vpliv Li_3AlF_6 kot sintrnega dodatka na strukturo in prevodnost keramičnih trdnih elektrolitov $Li_{0.25}La_{0.25}NbO_3$

Izvleček: Zaradi naraščajočega povpraševanja po sistemih za shranjevanje energije z visoko varnostjo in visoko energijsko gostoto so litijeve baterije v trdnem stanju (ASSLB) pritegnile veliko pozornosti zaradi svoje izjemne varnosti in potencialne visoke zmogljivosti. Med njimi je trdni elektrolit ključna sestavina. Ta študija sistematično preučuje učinke Li_3AlF_6 kot pomožnega sredstva na sintranje, kristalno strukturo, mikrostrukturo in elektrokemijsko zmogljivost keramike LLNO ($Li_{0.25}La_{0.25}NbO_3$). Keramični vzorci LLNO z različnimi stopnjami dopiranja z Li_3AlF_6 (0–8 mas. %) so bili pripravljeni s postopkom trdnofazne reakcije in sintrani pri 1050 °C in 1100 °C. Vzorci so bili karakterizirani z XRD, SEM, AC impedančno spektroskopijo in preskusom DC polarizacije. Rezultati kažejo, da Li_3AlF_6 znatno zniža temperaturo sintranja LLNO in pospeši proces zgoščevanja. Vendar prekomerno dopiranje (8 mas. %) vodi do nastanka nečistih faz, kot je AlF_3, poveča upornost na mejah zrn in zmanjša ionsko prevodnost. Vzorec s 5 mas. % Li_3AlF_6, sintran pri 1050 °C, kaže najboljšo splošno zmogljivost: ionsko prevodnost $2{,}08 \times 10^{-6}$ S·cm^{-1} in aktivacijsko energijo 0,340 eV. Čeprav je njegova prevodnost nekoliko nižja od prevodnosti čistega LLNO ($4{,}12 \times 10^{-6}$ S·cm^{-1}), sintranega pri 1100 °C, vnos Li_3AlF_6 ponuja izvedljivo pot za sintranje pri nizki temperaturi, kar je koristno za prihodnjo integracijo so-sintranja z elektrodnimi materiali.

Ključne besede: $Li_{0.25}La_{0.25}NbO_3$, Li_3AlF_6, dodatki za sintranje, keramika

** Corresponding Author's e-mail: huaianwwh@163.com, kongyazhou@hyit.edu.cn*

How to cite:
Y. Wang et al., "Effect of Li_3AlF_6 as Sintering-aids on the Structure and Conductivity of $Li_{0.25}La_{0.25}NbO_3$ Ceramic Solid Electrolytes", Inf. Midem-J. Microelectron. Electron. Compon. Mater., Vol. 56, No. 1(2026), pp. 37–45

1 Introduction

The escalating global demand for renewable energy and high-efficiency energy storage systems has positioned lithium-ion batteries (LIBs) as a cornerstone technology for portable electronics, electric vehicles, and large-scale grid storage [1-3]. However, conventional LIBs employing flammable organic liquid electrolytes pose significant safety risks, including leakage, combustion, and explosion, which hinder their applications in more demanding scenarios [4, 5]. In response to these challenges, all-solid-state lithium batteries (ASSLBs) have emerged as a promising next-generation energy storage technology due to their inherent safety, potential for higher energy density, and longer cycle life [6, 7].

The solid-state electrolyte (SSE) is the heart of an ASSLB, functioning not only as the Li^+ ion conductor but also as a separator to prevent short circuits between the cathode and anode. Thus, the properties of the SSE directly dictate the overall electrochemical performance of the battery [8, 9]. Among the various types of SSEs under investigation-including oxides, sulfides, polymers, and halides-oxide-based SSEs have attracted considerable attention owing to their excellent chemical stability, high mechanical strength, and wide electrochemical window [10, 11]. Prominent examples of oxide SSEs include the perovskite-type (e.g., $Li_{3x}La_{2/3-x}TiO_3$, LLTO), NASICON-type (e.g., $Li_{1+x}Al_xTi_{2-x}(PO_4)_3$, LATP), and garnet-type (e.g., $Li_7La_3Zr_2O_{12}$, LLZO) structures [12-14].

Within the perovskite family, lithium lanthanum niobate ($Li_xLa_{(1-x)/3}NbO_3$, often denoted as LLNO for specific compositions) has been recognized as a promising lithium-ion conductor. The composition $Li_{0.25}La_{0.25}NbO_3$ (LLNO), in particular, exhibits a relatively high bulk ionic conductivity and good thermal stability [15, 16]. Its structure provides interconnected pathways for lithium-ion migration, making it a candidate for ASSLB applications [17]. Despite these advantages, the practical application of LLNO, like many other oxide ceramics, faces several formidable challenges. A significant issue is the high grain boundary resistance, which often dominates the total resistance and limits the overall ionic conductivity [18]. Furthermore, the conventional synthesis of dense LLNO pellets typically requires high sintering temperatures (often 1100 °C) to achieve sufficient densification and grain growth [19, 20]. Such high-temperature processing is energy-intensive and can lead to undesirable phenomena, most notably lithium loss due to volatilization. Lithium deficiency can subsequently lead to the formation of secondary phases (e.g., $LaNbO_4$) and the creation of point defects, both of which can detrimentally affect the ionic transport properties and microstructural homogeneity of the final product [21, 22].

To address these issues, various strategies have been employed, including elemental doping, composite formation, and the use of sintering aids [23, 24]. The introduction of a sintering aid is a particularly effective approach for lowering the sintering temperature. These additives, often with lower melting points, can form a transient liquid phase during sintering. This liquid phase enhances mass transport, promotes particle rearrangement, and facilitates densification through solution-precipitation mechanisms, all at a reduced overall temperature [25, 26]. Coble et al. a theory has been proposed that adding MgO to Al_2O_3 can inhibit grain boundary migration and prevent secondary recrystallization, thereby obtaining transparent alumina [27]. Kenzhina et al. the addition of a small amount of ZrO_2 (1-5 mol%) can effectively inhibit the grain growth of $BaTiO_3$, enabling the ceramics to achieve densification at lower temperatures compared to pure $BaTiO_3$. This process results in a more uniform microstructure and superior dielectric properties [28].

Recently, lithium-containing halides and fluorides have been investigated as potent sintering aids for oxide SSEs [29, 30]. Among them, Li_3AlF_6, a lithium-aluminum fluoride compound, is highly attractive due to its relatively low melting point of approximately 790 °C [31]. During high-temperature treatment, Li_3AlF_6 can form a low-viscosity liquid that wets the oxide grain boundaries, effectively reducing the energy required for densification [32]. Moreover, as a lithium-rich compound, Li_3AlF_6 has the potential to supplement the lithium content in the matrix, potentially compensating for lithium loss during sintering and even modifying the grain boundary chemistry to enhance Li^+ transport [33, 34]. But the role and impact of Li_3AlF_6 in perovskite-type LLNO systems remain largely unexplored and poorly understood. A critical knowledge gap exists regarding how varying concentrations of Li_3AlF_6 influence the crystal structure, phase purity, microstructure evolution, and ultimately, the ionic conduction mechanism in LLNO. It is crucial to determine the optimal doping level, as an excess of Li_3AlF_6 could lead to the formation of resistive secondary phases (e.g., AlF_3, Al_2O_3) at the grain boundaries, which might impede Li^+ migration and degrade electrochemical performance [35]. A systematic investigation is therefore necessary to elucidate the underlying mechanisms and establish a composition-structure-property relationship in the LLNO-Li_3AlF_6 system.

In this study, we present a comprehensive investigation into the effects of Li_3AlF_6 doping on the sintering behavior, phase composition, microstructure, and

electrical properties of $Li_{0.25}La_{0.25}NbO_3$ (LLNO) perovskite solid electrolytes. A series of ceramic samples with nominal Li_3AlF_6 contents ranging from 0 to 8 wt.% were prepared via the solid-state reaction method and sintered at different temperatures. The crystal structures were characterized by X-ray diffraction (XRD), the microstructures were examined by scanning electron microscopy (SEM), and the electrical properties were evaluated by AC impedance spectroscopy and DC polarization measurements. Our work aims to unravel the dual role of Li_3AlF_6 as both a sintering aid and a microstructural modifier in the LLNO system. The findings provide valuable insights and a practical pathway for the low-temperature fabrication of high-performance LLNO-based solid electrolytes, which is a critical step towards their integration with electrode materials in commercially viable all-solid-state batteries.

2 Experimental

Ceramic compounds of the nominal chemical compositions $Li_{0.25}La_{0.25}NbO_3$ (LLNO) and LLNO doped with Li_3AlF_6 (1 wt.%, 3 wt.%, 5 wt.%, 8 wt.%) were prepared by solid-state reaction method from stoichiometric amounts of Li_2CO_3 (AR, 99.0%, Chengdu Cologne), La_2O_3 (99.9%, Aladdin), Nb_2O_5 (AR, 99.9%, Aladdin), Li_3AlF_6 (99.0%, Hubei Shishun). Excess Li_2CO_3 by 15 wt.%. Li_3AlF_6 powder was added to starting materials directly with the calculated amount. The raw material mixtures were homogenized via planetary ball milling (250 rpm, 4h) using ethanol (AR) as a liquid medium to ensure uniform particle distribution. Subsequently, the milled powders underwent pre-calcination in a box furnace at 900 °C for 12 h under ambient atmosphere to decompose carbonate and phosphate precursors. The calcined products were then subjected to secondary milling for 2 h by using agate mortar. The resulting powders were uniaxially pressed into pellets (10 MPa) using a hydraulic press. Finally, all pellets were sintered for 12 h at 1050 °C and 1100 °C. The LLNO doped with Li_3AlF_6 (3 wt.%, 5 wt.%, 8 wt.%) are melted on the sintering plate after sintering at 1100 °C. The detailed preparation conditions of all samples are shown in Table 1.

Table 1: Preparation conditions of the samples

Sample	Sintering temperature	Amount of Li_3AlF_6
1100 °C LLNO	1100 °C	0 wt.%
1100 °C LLNO-Li_3AlF_6 1%	1100 °C	1 wt.%
1050 °C LLNO	1050 °C	0 wt.%
1050 °C LLNO-Li_3AlF_6 1%	1050 °C	1 wt.%
1050 °C LLNO-Li_3AlF_6 3%	1050 °C	3 wt.%
1050 °C LLNO-Li_3AlF_6 5%	1050 °C	5 wt.%
1050 °C LLNO-Li_3AlF_6 8%	1050 °C	8 wt.%

In the end, we obtained seven intact samples of 1100 °C LLNO (sintered at 1100 °C), 1100 °C LLNO-Li_3AlF_6 1% (sintered at 1100 °C), 1050 °C LLNO (sintered at 1050 °C), 1050 °C LLNO-Li_3AlF_6 1% (sintered at 1050 °C), 1050 °C LLNO-Li_3AlF_6 3% (sintered at 1050 °C), 1050 °C LLNO-Li_3AlF_6 5% (sintered at 1050 °C), 1050 °C LLNO-Li_3AlF_6 8% (sintered at 1050 °C).

The phase composition of sintered pellets was determined by X-ray diffraction (XRD; Bruker D8 Advance) using Cu Kα radiation (λ = 1.5406 Å) and operating at a voltage and current of 40 kV and 40 mA, respectively. The data were collected over a 2θ range from 10° to 80°. Microstructure were characterized using scanning electron microscopy (SEM, Hitachi S-3000N). The ionic conductivity of the samples was measured using the HP 4192A impedance analyzer over a frequency range of 5 Hz to 13 MHz. The Alternating Current (AC) impedance spectra were recorded at temperatures from 25 °C to 100 °C to determine activation energies. Electronic conductivity was evaluated by Direct Current (DC) polarization (ADCMT 6243R) under a constant 5 V bias applied for 6000 s at 25 °C. Both AC impedance measurements and DC polarization tests utilized electronically conductive graphite electrodes. Graphite was uniformly coated onto both sides of the electrolyte pellets to serve as electrodes. As graphite conducts electrons but cannot transport lithium ions, it constitutes an excellent test electrode material for this study.

The density of ceramic samples was determined via the Archimedes principle (water displacement method). Prior to measurement, the samples were cleaned to remove surface contaminants. The dry mass (m_1) was measured using an analytical balance by suspending the sample in a corrosion-resistant wire basket. For the measurement of the apparent mass in liquid (m_2), the entire setup was fully immersed in temperature-controlled (25.0 ± 0.1 °C) deionized water. Bubbles adhering to the sample surface were removed by gentle agitation. The sample was suspended at a depth of ≥20 mm below the water surface to avoid meniscus effects. With the density of water (ρ_1) taken as 1 g·cm^{-3}, the density of the ceramic samples (ρ) was calculated using the following formula:

$$\rho = \frac{m_1}{m_1 - m_2}\rho_1 \quad (1)$$

3 Results and discussion

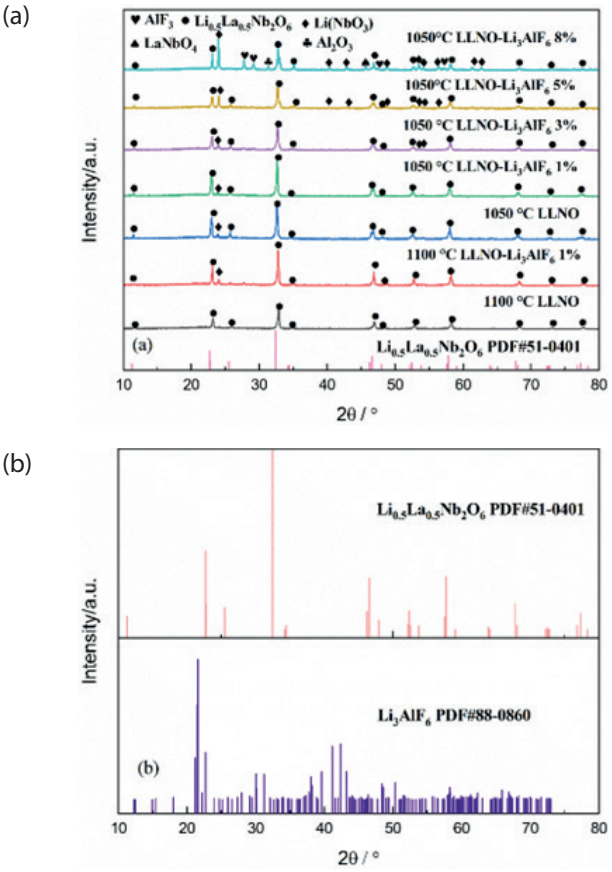

Figure 1: (a) XRD result of ceramic pellets sintered at 1050 °C and 1100 °C, (b) reference pattern of $Li_{0.5}La_{0.5}Nb_2O_6$ and Li_3AlF_6.

Fig.1. (a) shows the XRD patterns of $Li_{0.25}La_{0.25}NbO_3$ (LLNO) doped with varying contents of Li_3AlF_6 at 1050 °C and 1100 °C, compared with the standard XRD pattern of $Li_{0.5}La_{0.5}Nb_2O_6$ (PDF#51-0401). The main diffraction peaks for all samples belong to cubic perovskite structure. Minor peaks from secondary phases such as $Li(NbO_3)$ (PDF#70-4306), Al_2O_3 (PDF#86-1407), $LaNbO_4$ (PDF#85-1107) and AlF_3 (PDF#47-1659) are confirmed in LLNO sintered with varying contents of Li_3AlF_6. The peak intensity of $Li(NbO_3)$ and AlF_3 in LLNO sintered with Li_3AlF_6 is found to be much larger than in LLNO sintered without Li_3AlF_6. The result suggests that during high temperature sintering, Li loss in LLNO and Li_3AlF_6 is easily occurred and results into the formation of impurity phase such as $Li(NbO_3)$ and AlF_3. Specifically, $Li(NbO_3)$ was detected in all LLNO composites containing ≥1 wt.% Li_3AlF_6, while AlF_3 was additionally observed in the sample with 8 wt.% Li_3AlF_6. The diffraction peak intensities for both impurity phases increased with the amount of added Li_3AlF_6. It can be seen that the diffraction peaks of all samples shift to higher angles compared with the standard XRD pattern of $Li_{0.5}La_{0.5}Nb_2O_6$. This shift is commonly interpreted as lattice contraction, though further structural analysis would be required to confirm this hypothesis. Thus, taking into consideration the results of XRD mentioned above, it may be concluded that the high contents of Li_3AlF_6 lead to more impurity and the peak intensity for LLNO phase is greatly reduced.

The Li_3AlF_6 (3 wt.%, 5 wt.%, 8 wt.%) modified LLNO ceramic pellet sintered at 1100 °C is melted on the sintering plate, which leads to the difficulty in obtaining an intact pellet for characterization. In this system, Li_3AlF_6 acts as a sintering aid by forming a liquid phase that facilitates densification at lower temperatures. Its melting point is 790 °C, and we observed evidence of melting in LLNO doped with Li_3AlF_6 (3 wt.%, 5 wt.%, 8 wt.%) samples at sintering temperatures of 1050 °C and 1100 °C. This liquid phase promotes ceramic phase formation and significantly reduces the required sintering temperature for LLNO. Consequently, no residual Li_3AlF_6 diffraction peaks are detected in the final composite ceramics (Fig. 1. (b)), indicating its complete reaction or dissolution during the process.

Fig. 2 illustrates the fracture surface morphology of the ceramic samples as observed by SEM. As shown in Table 1, the density of all ceramic samples falls within the range of 4.6-4.8 $g{\cdot}cm^{-3}$. All ceramic samples in Fig. 2 demonstrate a dense microstructure with minimal large-scale porosity. It indicates that the synthesized ceramic samples exhibit an excellent degree of densification. As shown in Fig. 2. (d)-(g), we observed that some grains failed to develop, which may be attributed to the segregation of impurities at the grain boundaries during the sintering process, forming low-melting-point glass phases or secondary phase particles. These substances pin the grain boundaries like "nails", hindering their movement and thereby inhibiting normal grain growth. As shown in Fig. 2. (a) and (c), we found that after reducing the sintering temperature by 50 °C, the LLNO exhibited a plate-like tetragonal structure. This change can be attributed to the deteriorated kinetic conditions for grain growth resulting from the lower sintering temperature. As shown in Fig. 2. (a)-(g), a multitude of fine impurity particles can be observed, which are attributed to Li_3AlF_6 doping. In summary, the perovskite structure of LLNO remained largely unchanged with either lower temperature or higher Li_3AlF_6 doping levels.

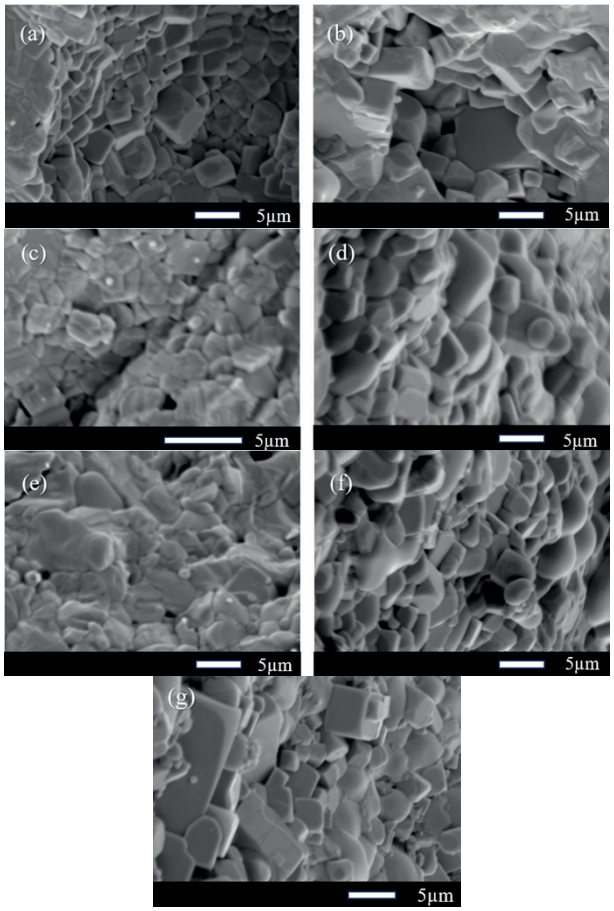

Figure 2: SEM images of fracture surface of the samples: (a) 1100 °C LLNO, (b) 1100 °C LLNO-Li_3AlF_6 1%, (c) 1050 °C LLNO, (d) 1050°C LLNO-Li_3AlF_6 1%, (e) 1050 °C LLNO-Li_3AlF_6 3%, (f) 1050 °C LLNO-Li_3AlF_6 5%, (g) 1050 °C LLNO-Li_3AlF_6 8%.

Typical impedance plots of LLNO and LLNO doped with varying contents of Li_3AlF_6 at 25 °C are shown in Fig. 3. (a). The semicircle by the grain boundary contribution is observed at higher frequency range and a straight line at lower frequency range. The ideal impedance spectrum of solid electrolyte is composed by grains and grain boundaries and ion-blocking electrodes. It is identified in the impedance spectra that the semicircle represents the relaxation process in the grain boundaries, and the straight line is attributable to the electrode polarization in the blocking electrodes. The resistance and conductivity of ceramic samples are listed in Table 1 at room temperature.

The highest conductivity of ceramic pellets sintered at 1050 °C is 2.08×10^{-6} S·cm^{-1} when LLNO doped with 5 wt.% Li_3AlF_6, which is larger than that of pure LLNO sintered at 1050 °C is 1.16×10^{-6} S·cm^{-1}. As the sintering temperature decreases from 1100 °C to 1050 °C, LLNO and LLNO-Li_3AlF_6 1% resistance increases from 50-100 kΩ to 150-250 kΩ. The reduction of resistance

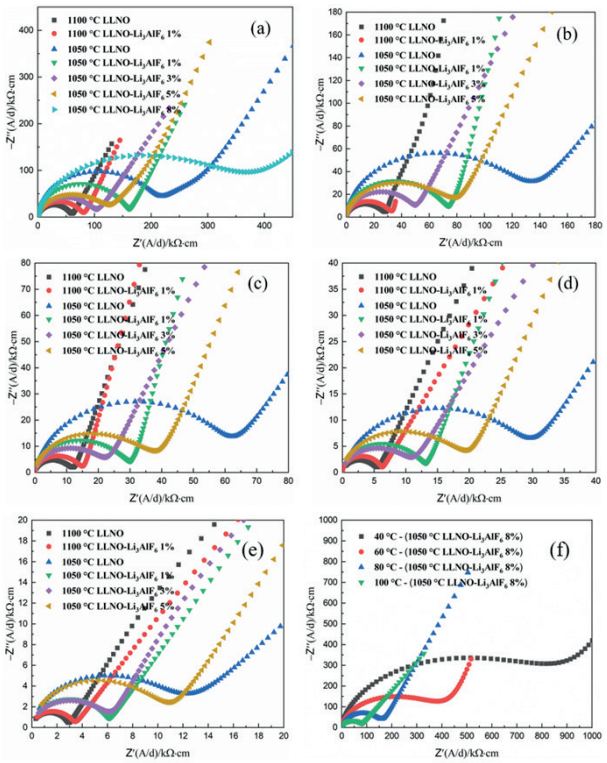

Figure 3: Nyquist plots measured under different conditions (samples were sintered at 1050 °C and 1100 °C): ceramic pellets measured at (a) 25 °C, (b) 40 °C, (c) 60 °C, (d) 80 °C, (e) 100 °C, and (f) LLNO samples with 8 wt.% Li_3AlF_6 measured at different temperatures.

with increasing the sintering temperature below 1100 °C is caused by the densification and improvements in intergranular connectivity. At the sintering temperature of 1050 °C, however, LLNO-Li_3AlF_6 8% resistance is estimated to be approximately 400 kΩ and becomes larger than the other ceramic samples. Increase in resistance observed in the sample sintered at 1050 °C may be caused by the formation of very small amounts of secondary phases formed on the LLNO grain surface due to excess doped with Li_3AlF_6 and Li volatilization.

Fig. 3. (b)-(f) presents the Nyquist plots for the electrochemical impedance of all ceramic samples across different temperatures. These plots reveal two key trends: first, the overall impedance of the samples decreases significantly as temperature increases; second, the linear low-frequency tails of the plots gradually extend outward with a slope approaching 45 degrees as the temperature rises. As shown in Fig. 3. (f), it is observed that while the impedance of LLNO-Li_3AlF_6 8% is strongly temperature-dependent, its values are markedly elevated compared to the other ceramic samples throughout the measured temperature range. As shown in Table 1, the conductivity of LLNO-Li_3AlF_6 8% is 5.93×10^{-7} S·cm^{-1}, which is lower by one order of magnitude than that of the other ceramic samples (10^{-6} S·cm^{-}

[1]). We believed that the secondary phases contained in LLNO with 8 wt.% excess Li_3AlF_6 severely interfere with Li ion conduction at grain boundaries.

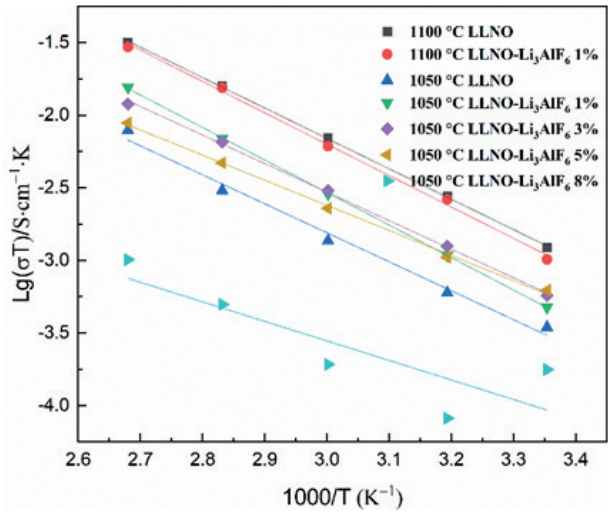

Figure 4: Arrhenius diagram of ceramic pellets (color online)

Fig. 4 shows variation of the product of σ and measurement temperature T for all sintered LLNO as a function of inverse of temperature T. E_a of each sample can be estimated from the slope of σT in Fig. 4. E_a tends to decrease with increasing the contents of Li_3AlF_6 and shows the minimum (= 0.266 eV). However, LLNO-Li_3AlF_6 8% the fitted line does not exactly correspond to the data points and shows significant deviations. The fitted curves for the other six sets of ceramic samples correspond well with their respective data points. The observed reduction in activation energy with higher Li_3AlF_6 content is mainly due to the properties of Li_3AlF_6. It provides a significant reservoir of highly mobile lithium ions. As its concentration increases, both the total lithium-ion content and their electrochemical activity within the composite rise. This creates more facile conduction pathways, effectively lowering the energy barrier (activation energy) for ion transport through the ceramic sample. As show in Fig. 4 and Table 1, as the sintering temperature decreases from 1100 °C to 1050 °C, it was observed that the activation energy of LLNO decreased by approximately 0.02 eV, whereas that of LLNO-Li_3AlF_6 1% increased by about 0.02 eV. Interestingly, despite these opposing changes in activation energy, the conductivity was reduced by 2-3 times for both ceramic samples. This suggests that the sintering temperature, whether at 1050 °C or 1100 °C, has a negligible effect on the activation energy for both LLNO and LLNO-Li_3AlF_6 1%. These data of the ceramic samples demonstrate that although LLNO-Li_3AlF_6 8% has the lowest activation energy, it is unstable. Among the remaining ceramic samples, LLNO-Li_3AlF_6 5% exhibits a relatively low activation energy (= 0.340 eV) along with good stability.

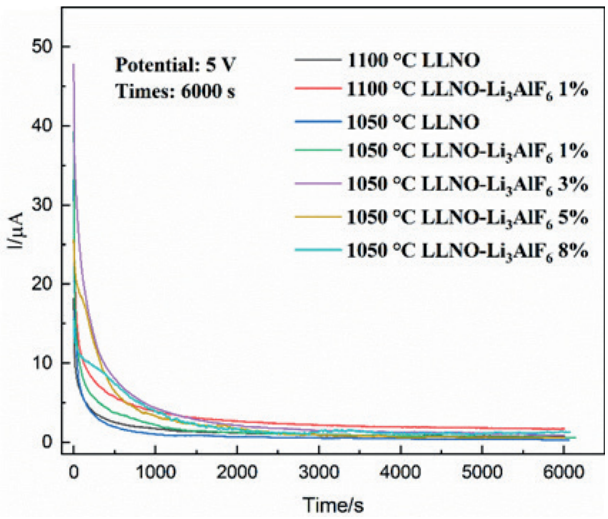

Figure 5: DC polarization plots of ceramic pellets

The result of the DC polarization test is shown in Fig. 5. For all samples, after approximately 2000s, the current reached a steady state, and the ionic current was completely blocked. For the samples of LLNO-Li_3AlF_6 8%, the current fluctuates slightly during the DC polarization test but the overall is stable. Electronic conductivity can be determined from applied DC voltage (= 5 V), steady state current and geometrical parameters (surface area and thickness) of ceramic sample. As shown in Fig. 5 and Table 1, the calculated electronic

Table 2: Density, total resistance, conductivity and conductivity electronic at room temperature, and activation energy of the ceramic samples

Sample	Density/ g·cm^{-3}	R_{total}/Ω	$\sigma_{total\text{-}25\ °C}$/ S·cm^{-1}	$\sigma_{ele\text{-}25\ °C}$/ S·cm^{-1}	Ea/ eV
1100 °C LLNO	4.646	59915.29	4.12×10^{-6}	3.85×10^{-8}	0.414
1100 °C LLNO-Li_3AlF_6 1%	4.689	80951.65	3.40×10^{-6}	1.04×10^{-7}	0.427
1050 °C LLNO	4.595	219649.70	1.16×10^{-6}	1.99×10^{-8}	0.395
1050 °C LLNO-Li_3AlF_6 1%	4.739	161251.00	1.59×10^{-6}	4.07×10^{-8}	0.443
1050 °C LLNO-Li_3AlF_6 3%	4.830	103506.90	1.91×10^{-6}	3.97×10^{-8}	0.389
1050 °C LLNO-Li_3AlF_6 5%	4.701	123761.90	2.08×10^{-6}	3.04×10^{-8}	0.340
1050 °C LLNO-Li_3AlF_6 8%	4.652	374315.40	5.93×10^{-7}	4.44×10^{-8}	0.266

conductivity of all ceramic samples are 1-2 orders of magnitude lower than the corresponding conductivity. When the sintering temperature was reduced by 50 °C, we found that the electronic conductivity of LLNO (1.99×10^{-8} S·cm^{-1}) decreased by a factor of 3 compared to that of LLNO sintered at 1100 °C (3.85×10^{-8} S·cm^{-1}), while the electronic conductivity of LLNO-Li_3AlF_6 1% (4.07×10^{-8} S·cm^{-1}) dropped by approximately an order of magnitude relative to its 1100 °C (1.04×10^{-7} S·cm^{-1}) counterpart. Among all samples sintered at 1050°C, LLNO-Li_3AlF_6 8% (4.44×10^{-8} S·cm^{-1}) exhibited the highest electronic conductivity, while LLNO showed the lowest (1.99×10^{-8} S·cm^{-1}). This indicates that Li_3AlF_6 doping leads to an increase in electronic conductivity. However, as shown in table 1, as the Li_3AlF_6 doping content increased from 1% to 5%, the electronic conductivity decreased (4.07×10^{-8} S·cm^{-1} to 3.04×10^{-8} S·cm^{-1}).

4 Conclusions

The study investigates the crystal structure and electrochemical properties of the perovskite-type solid electrolyte $Li_{0.25}La_{0.25}NbO_3$ (LLNO) doped with varying contents of Li_3AlF_6. As deduced from the measurements of AC impedance, the temperature dependence of the conductivity follows an Arrhenius law. The ionic conductivity of LLNO sintered at 1050 °C reaches a maximum of 2.08×10^{-6} S·cm^{-1} with 5 wt.% Li_3AlF_6 addition, accompanied by a favorable activation energy of 0.340 eV. Although this value is lower than the 4.12×10^{-6} S·cm^{-1} achieved by pure LLNO sintered at 1100 °C, the role of Li_3AlF_6 is significant. Firstly, it systematically enhances ionic conductivity at 1050 °C, with performance improving up to the 5 wt.% doping level. More importantly, Li_3AlF_6 acts as an effective sintering aid, reducing the required processing temperature by 50 °C. This reduction is highly advantageous for the future co-sintering of LLNO solid electrolytes with electrode materials in the fabrication of all-solid-state lithium batteries. This study provides a potential method for future researchers to cut down the sintering temperature.

5 Acknowledgement

This work was supported by the Natural Science Foundation of the Higher Education Institutions of Jiangsu Province (23KJB450001), Foundation of Key Laboratory for Palygorskite Science, and Applied Technology of Jiangsu Province (HPZ202201), Huaiyin Institute of Technology College Students' Innovation and Entrepreneurship Training Program Project (X202511049244).

6 Conflict of interest

No financial or interpersonal conflicts have been reported by the authors that would have affected the study's finding.

7 References

1. J. B. Goodenough, and K.-S. Park, "The Li-Ion Rechargeable Battery: A Perspective," J. Am. Chem. Soc., vol. 135, no. 4, pp. 1167-1176, Jan. 2013, https://doi.org/10.1021/ja3091438.
2. M. Armand, and J.-M. Tarascon, "Building better batteries", Nature, vol. 451, no. 7149, pp. 652-657, Feb. 2008, https://doi.org/10.1038/451652a.
3. V. Ambrozic, M. Breznik, M. Nemec, "Operation of Permanent Magnet Synchronous Motor after Open-circuit Battery Supply Fault", Inform. MIDEM, vol. 52, no. 1, pp 17-27, 2022, https://doi.org/10.33180/InfMIDEM2022.103.
4. D. H. S. Tan, E. A. Wu, H. Nguyen, Z. Chen, M. A. T. Marple, J.-M. Doux, et al., "Elucidating Reversible Electrochemical Redox of Li_6PS_5Cl Solid Electrolyte," ACS Energy Lett., vol. 4, no. 10, pp. 2418-2427, Aug. 2019, https://doi.org/10.1021/acsenergylett.9b01693.
5. W. Xu, J. Wang, F. Ding, X. Chen, E. Nasybulin, Y. Zhang, and J-G. Zhang, "Lithium metal anodes for rechargeable batteries," Energy Environ. Sci., vol.7, no. 2, pp. 513-537, Oct. 2013, https://doi.org/10.1039/C3EE40795K.
6. A. Manthiram, X. Yu, and S. Wang, "Lithium battery chemistries enabled by solid-state electrolytes," Nat. Rev. Mater., vol. 2, no. 4, pp. 16103, Feb. 2017, https://doi.org/10.1038/natrevmats.2016.103.
7. Y. Kato, S. Hori, T. Saito, K. Suzuki, M. Hirayama, A. Mitsui, M. Yonemura, H. Iba & R. Kanno, "High-power all-solid-state batteries using sulfide superionic conductors," Nat. Energy, vol. 1, no. 4, pp. 16030, Mar. 2016, https://doi.org/10.1038/nenergy.2016.30.
8. J. C. Bachman, S. Muy, A. Grimaud, H.-H. Chang, N. Pour, S. F. Lux, O. Paschos, F. Maglia, S. Lupart, P. Lamp, L. Giordano, and Y. Shao-Horn, "Inorganic Solid-State Electrolytes for Lithium Batteries: Mechanisms and Properties Governing Ion Conduction," Chem. Rev., vol. 116, no. 1, pp. 140-162, Jan. 2016, https://doi.org/10.1021/acs.chemrev.5b00563
9. Q. Liu, Z. Geng, C. Han, Y. Fu, S. Li, Y.-b. He, F. Kang, B. Li, "Challenges and perspectives of garnet solid electrolytes for all solid-state lithium batteries," J.

Power Sources, vol. 389, pp. 120-134, Jun. 2018, https://doi.org/10.1016/j.jpowsour.2018.04.019
10. V. Thangadurai, S. Narayanan, and D. Pinzaru, "Garnet-type solid-state fast Li ion conductors for Li batteries: critical review," Chem. Soc. Rev., vol. 43, no. 13, pp. 4714-4727, May 2014, https://doi.org/10.1039/C4CS00020J.
11. X. Yao, B. Huang, J. Yin, G. Peng, Z. Huang, C. Gao, D. Liu, and X. Xu, "All-Solid-State Lithium Batteries with Inorganic Solid Electrolytes: Review of Fundamental Science," Chin. Phys. B, vol. 25, no. 1, pp. 018802, Jan. 2016, https://doi.org/10.1088/1674-1056/25/1/018802.
12. Y. Inaguma, C. Liquan, M. Itoh, T. Nakamura, T. Uchida, H. Ikuta, M. Wakihara, "High ionic conductivity in lithium lanthanum titanate," Solid State Commun., vol. 86, no. 10, pp. 689-693, Jun 1993, https://doi.org/10.1016/0038-1098(93)90841-A.
13. H. Aono, E. Sugimoto, Y. Sadacka, N. Imanaka, and G. Adachi, "Ionic Conductivity of the Lithium Titanium Phosphate ($Li_{1+x}M_xTi_{2-x}(PO_4)_3$, M = Al, Sc, Y, and La) Systems", J. Electrochem. Soc., vol. 136, no. 2, pp. 590-591, Feb. 1989, https://doi.org/10.1149/1.2096693.
14. R. Murugan, V. Thangadurai, and W. Weppner, "Fast Lithium Ion Conduction in Garnet-Type $Li_7La_3Zr_2O_{12}$," Angew. Chem. Int. Ed., vol. 46, no. 41, pp. 7778-7781, 2007, https://doi.org/10.1002/anie.200701144.
15. S. Stramare, V. Thangadurai, and W. Weppner, "Lithium Lanthanum Titanates: A Review," Chem. Mater., vol. 15, no. 21, pp. 3974-3990, Sep. 2003, https://doi.org/10.1021/cm0300516.
16. Y. Li, J.-T. Han, C.-A. Wang, H. Xie, and J. B. Goodenough, "Optimizing Li+ conductivity in a garnet framework," J. Mater. Chem., vol. 22, no. 30, pp. 15357-15361, 2012, https://doi.org/10.1039/c2jm31413d.
17. J-Q. Zheng, Y-F. Li, R. Yang, G. Li, X-K. Ding, "Lithium ion conductivity in the solid electrolytes $(Li_{0.25}La_{0.25})_{1-x}M_{0.5x}NbO_3$ (M=Sr, Ba, Ca, x=0.125) with perovskite-type structure," Ceram. Int., vol. 43, no. 2, pp. 1716-1721, Feb. 2017, https://doi.org/10.1016/j.ceramint.2016.08.144.
18. N. J. J. de Klerk and M. Wagemaker, "Space-Charge Layers in All-Solid-State Batteries; Important or Negligible?," ACS Appl. Energy Mater., vol. 1, no. 11, pp. 5609-5618, Nov. 2018, https://doi.org/10.1021/acsaem.8b01141.
19. Y. Ma, Y. Wei, M. K, R. Li, D. Yan, D. Wang and E. Liu, "Effect of sintering temperature on microstructure and electrical properties of $Na_{0.5}Bi_{0.47}Sr_{0.02}TiO_{3-\delta}$ ceramics," Mater. Res. Express, vol. 11, no. 5, pp. 933-941, May. 2024, https://doi.org/10.1088/2053-1591/ad425e.
20. X. Gao, C. J. Fisher, Y. H. Ikuhara, Y. Fujiwara, S. Kobayashi, H. Moriwake, A. Kuwabara, K. Hoshikawa, K. Kohama, H. Iba and Y. Ikuhara, "Cation ordering in A-site-deficient Li-ion conducting perovskites $La_{(1-x)/3}Li_xNbO_3$," J. Mater. Chem. A, vol. 3, no. 3, pp. 3351-3359, 2015, https://doi.org/10.1039/C4TA07040B.
21. S. Ohta, T. Kobayashi, and T. Asaoka, "High lithium ionic conductivity in the garnet-type oxide $Li_{7-x}La_3(Zr_{2-x}, Nb_x)O_{12}$ (X=0-2)," J. Power Sources, vol. 196, no. 6, pp. 3342-3345, Mar. 2011, https://doi.org/10.1016/j.jpowsour.2010.11.089.
22. C. L. Tsai, V. Roddatis, C. V. Chandran, Q. Ma, S. Uhlenbruck, M. Bram, P. Heitjans, and O. Guillon, "$Li_7La_3Zr_2O_{12}$ Interface Modification for Li Dendrite Prevention," ACS Appl. Mater. Interfaces, vol. 8, no. 16, pp. 10617-10626, Apr. 2016, https://doi.org/10.1021/acsami.6b00831.
23. T. Thompson, S. Yu, L. Williams, R. D. Schmidt, R. Garcia-Mendez, J. Wolfenstine, J. L. Allen, E. Kioupakis, D. J. Siegel, and J. Sakamoto, "Electrochemical Window of the Li-Ion Solid Electrolyte $Li_7La_3Zr_2O_{12}$," ACS Energy Lett., vol. 2, no. 2, pp. 462-468, Jan. 2017, https://doi.org/10.1021/acsenergylett.6b00593.
24. Y. Shao, H. Wang, Z. Gong, D. Wang, B. Zheng, J. Zhu, Y-S. Hu, X. Guo, H. Li, X. Huang, Y. Yang, C-W. Nan, and L. Chen, "Drawing a Soft Interface: An Effective Interfacial Modification Strategy for Garnet-Type Solid-State Li Batteries," ACS Energy Lett., vol. 3, no. 6, pp. 1212-1218, May 2018, https://doi.org/10.1021/acsenergylett.8b00453.
25. R-H. Shin, S-I. Son, S-M. Lee, Y. S. Han, Y. D. Kim, S-S. Ryu, "Effect of Li_3BO_3 additive on the densification and ionic conductivity of garnet-type $Li_7La_3Zr_2O_{12}$ solid electrolytes of All-Solid-State Lithium-Ion Batteries," J. Korean. Ceram. Soc., vol. 53, no. 6, pp. 712-718, 2016, https://doi.org/10.4191/kcers.2016.53.6.712.
26. H. El Shinawi and J. Janek, "Stabilization of cubic lithium-stuffed garnets of the type '$Li_7La_3Zr_2O_{12}$' by addition of gallium," J. Power Sources, vol. 225, pp. 13-19, Mar. 2013, https://doi.org/10.1016/j.jpowsour.2012.09.111.
27. R. L. Coble, "Sintering Crystalline Solids. II. Experimental Test of Diffusion Models in Powder Compacts", J. Appl. Phys., vol. 32, no. 5, pp. 793-799, May. 1961, https://doi.org/10.1063/1.1736108.
28. I. E. Kenzhina, A. L. Kozlovskiy, N. O. Volodina, R. I. Shakirzyanov, Y. A. Garanin, S. A. Maznykh, K. M. Makhanov, A. U. Tolenova, M. Begentayev, S. K. Askerbekov, P. A. Blynskiy, Z. A. Zaurbekova, "Low-temperature sintering of zirconia-based ceramic composites for capacitor applications", Part A, vol. 51, no. 21, pp. 33428-33440, Sep. 2025, https://doi.org/10.1016/j.ceramint.2025.05.075.

29. Y. Zhu, X. He, and Y. Mo, "Origin of Outstanding Stability in the Lithium Solid Electrolyte Materials: Insights from Thermodynamic Analyses Based on First-Principles Calculations," ACS Appl. Mater. Interfaces, vol. 7, no. 42, pp. 23685-23693, Oct. 2015, https://doi.org/10.1021/acsami.5b07517.
30. H. Yamada, T. Ito, R. H. Basappa, "Sintering Mechanisms of High-Performance Garnet-type Solid Electrolyte Densified by Spark Plasma Sintering" Electrochim. Acta, vol. 222, pp. 648-656, Dec. 2016, https://doi.org/10.1016/j.electacta.2016.11.020.
31. G. Garton, B. M. Wanklyn, "Reinvestigation of the System Na_3AlF_6-Li_3AlF_6," J. Am. Ceram. Soc., vol. 50, no. 8, pp. 395-399, Aug. 1967, https://doi.org/10.1111/j.1151-2916.1967.tb15142.x.
32. S. S. Berbano, J. Guo, H. Guo, M. T. Lanagan, C. A. Randall, "Cold sintering process of $Li_{1.5}Al_{0.5}Ge_{1.5}(PO_4)_3$ solid electrolyte," J. Am. Ceram. Soc., vol. 100, no. 5, pp. 2123-2135, May 2017, https://doi.org/10.1111/jace.14727.
33. Y. Liu, S. Zhao, L. Wang, Y. Li, H. Zhou, Z. He, W. Meng, L. Dai, "Effect of LiF on the ion conductivity and sinterability of $(Al_{0.2}Zr_{0.8})_{20/19}Nb(PO_4)_3$ solid electrolyte" J. Alloy. Compd., vol. 851, pp. 156337, Jan. 2021, https://doi.org/10.1016/j.jallcom.2020.15633734.
34. Z. Gao, H. Sun, L. Fu, F. Ye, Y. Zhang, W. Luo, Y. Huang, "Promises, Challenges, and Recent Progress of Inorganic Solid-State Electrolytes for All-Solid-State Lithium Batteries," Adv. Mater., vol. 30, no. 17, pp. 1705702, Apr. 2018, https://doi.org/10.1002/adma.201705702.
35. K. Park, B. C. Yu, J. W. Jung, Y. Li, W. Zhou, H. Gao, S. Son, and J. B. Goodenough, "Electrochemical Nature of the Cathode Interface for a Solid-State Lithium-Ion Battery: Interface between $LiCoO_2$ and Garnet-$Li_7La_3Zr_2O_{12}$," Chem. Mater., vol. 28, no. 21, pp. 8051-8059, Nov. 2016, https://doi.org/10.1021/acs.chemmater.6b03870.

Arrived: 28. 11. 2025
Accepted: 14. 02. 2026